Optical bistability in Er-Yb codoped phosphate glass microspheres at room temperature

Jonathan M. Ward[a)]
Department of Applied Physics and Instrumentation, Cork Institute of Technology, Bishopstown, Cork, Ireland
and Photonics Centre, Tyndall National Institute, Prospect Row, Cork, Ireland

Danny G. O'Shea
Physics Department, University College Cork, Ireland
and Photonics Centre, Tyndall National Institute, Prospect Row, Cork, Ireland

Brian J. Shortt
Department of Applied Physics and Instrumentation, Cork Institute of Technology, Bishopstown, Cork, Ireland
and Photonics Centre, Tyndall National Institute, Prospect Row, Cork, Ireland

Síle Nic Chormaic
Physics Department, University College Cork, Ireland
and Photonics Centre, Tyndall National Institute, Prospect Row, Cork, Ireland

(Received 15 February 2007; accepted 31 May 2007; published online 20 July 2007)

We experimentally demonstrate optical bistability in Er^{3+}-Yb^{3+} phosphate glass microspheres at 295 K. Bistability is associated with both Er^{3+} fluorescence and lasing behavior, and chromatic switching. The chromatic switching results from an intrinsic mechanism exploiting the thermal coupling of closely spaced energy levels, and occurs simultaneously with the intensity switching. A contrast ratio of 2.8 has been obtained for chromatic switching. The intensity switching shows ratios of 21 for 520 nm and 11 for 660 nm fluorescence emissions, and 11 for IR lasing at 1.5 μm. Concurrent with these observations, we investigate a temperature-dependent absorption of pump power, which exhibits bistable behavior. The influences of the host matrix on lasing and fluorescence mechanisms are highlighted. © *2007 American Institute of Physics*.
[DOI: 10.1063/1.2753591]

I. INTRODUCTION

Optical bistability (OB) in a sodium vapor was reported by Gibbs in 1976[1] and, since then, numerous other materials exhibiting the phenomenon have been studied, including Yb^{3+} doped glasses and crystals, and semiconductors.[2–8] The mechanisms responsible for nonlinearity in glasses and crystals are varied, with many requiring cryogenic temperatures (typically <40 K) to maintain the necessary low atomic decay rates in Yb^{3+} dimer and monomer systems.[3] Alternative and more easily achievable mechanisms include photon avalanche and thermal avalanche,[2,5] suggesting that a wider range of materials can exhibit OB at room temperature and above. However, no evidence of OB through these mechanisms in this temperature range has yet been observed. Bistable sensitized luminescence in Er-Yb:$CsCdBr_3$ was shown by Redmond and Rand,[3] and, subsequently, by Ródenas *et al.*[4] in a Nd-Yb codoped crystal. They also described *chromatic switching* in addition to the more traditional *intensity switching*, though both mechanisms required temperatures well below room temperature. In chromatic switching, the wavelengths of light emitted from an optically pumped sample change abruptly as a function of pump power. In contrast, for intensity switching, the output intensity at any particular wavelength changes abruptly as a function of pump power. To date, OB has also been predicted and observed in Yb^{3+} doped oxide crystals, Cr-doped $LiSrGaF_6$ and $LiSrAlF_6$ crystals,[5] Sm^{3+} doped glass microspheres,[6] and Tm^{3+}-Yb^{3+} codoped glass.[7] The later system exhibited multiple hysteresis loops in the fluorescence intensity at room temperature.

The interest in studying micron-sized spherical cavities stems from the potential they offer as components for experiments ranging from the very applied realization of all-optical networks to fundamental quantum optics experiments, whereby the microspheres can be used as ultrahigh Q cavities for measurements based on the principles of cavity quantum electrodynamics.[9] Such microcavities can be either active or passive depending on the material used. For example, a sphere doped with the triply ionized rare-earth ions Er^{3+} can yield fluorescence emissions ranging from UV to IR through various upconversion mechanisms,[10,11] due to the close proximity of the numerous energy levels in the ion. Microcavities that exhibit optical bistability are interesting for generating optical switches for all-optical computing, and miniature C-band laser sources are important for telecommunications applications.[12] These factors have resulted in significant research focusing on the characterization of microcavities in recent years.

The concept of an Er^{3+}-Yb^{3+} codoped glass laser was demonstrated[13] in 1965 as a means of optimizing the Er^{3+}

[a)]Electronic mail: Jonathan.ward@cit.ie

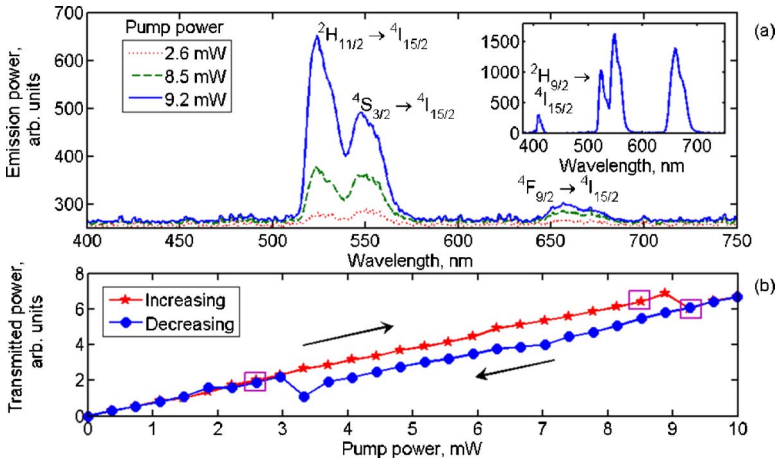

FIG. 1. (Color online) (a) Upconversion fluorescence spectrum for three different pump powers in a 50-μm-diam IOG-2 microsphere. The inset shows an additional weak violet emission from a 35-μm-diam microsphere, observable when no lasing emission at 1.5 μm is present and for a pump power of 8 mW. The violet emission has been scaled up by a factor of 5 for clarity. The ratio of the emission powers from the $^2H_{11/2}$ to $^4S_{3/2}$ levels for a pump power of 9.2 mW is 1.34. (b) Transmitted power past the taper-sphere junction for the 50 μm sphere as shown in (a). The three spectra in (a) correspond with the three highlighted data points (□) in (b).

emission cross section while simultaneously ensuring an optimum Yb^{3+} absorption cross section.[14] This overlap alleviates the difficulty of trying to directly pump the narrow Er^{3+} absorption band. Phosphate glass has been investigated as a host matrix for rare-earth ions due to its favorable properties, such as (i) the possibility of obtaining large dopant concentrations (up to 1.8×10^{21} ions/cm^3 for Yb^{3+}, and $\sim10^{19}$ ions/cm^3 for Er^{3+}) compared to silicate, borate, and fluoride glasses, (ii) its large absorption band in the near-infrared region, (iii) its large emission cross section at 1.5 μm, and (iv) the low back energy transfer from Er^{3+} ions to Yb^{3+} ions.[15–17] The spectral characteristics are also especially beneficial for C-band lasing; the intermediate lasing level $^4I_{11/2}$ has a high nonradiative relaxation rate (<1 μs lifetime, maximum phonon energy of 1300 cm^{-1}) to the $^4I_{13/2}$ level compared with silica (maximum phonon energy of 1190 cm^{-1}), and the long lifetime of the $^4I_{13/2}$ level of about 8.45 ms facilitates population inversion and high gain.[12] The larger phonon energy of phosphate glass has a negative effect on the upconversion efficiency compared to fluoride glass (with a maximum phonon energy of 600 cm^{-1}). This, however, is counterbalanced by the large dopant concentrations and wide absorption cross section of the Yb^{3+} sensitizer. In addition, phosphate glass has better optomechanical properties compared to other glasses used for OB, such as $CsCdBr_3$.

Here, we report on the simultaneous observation of chromatic and intensity OB in phosphate glass (Schott IOG-2) at room temperature. We present experimental results on lasing around 1550 nm and propose suitable upconversion mechanisms for the observed three color emission bands. Optical bistability previously demonstrated in passive silica[9,18] and silicon[8] resonators was attributed to nonlinearities arising from the Kerr effect or thermo-optic effect of the resonance line, together with high Q factors ($Q>10^8$) and a tunable, narrow linewidth laser. The results presented here clearly show that IOG-2 microspheres exhibit bistable switching behavior under vastly different conditions; we use microspheres with relatively high loaded cavity Q's typically 1×10^7, and the pump laser has a linewidth of 1 nm and is not locked to individual cavity resonances. For clarity, our results are organized in two sections: fluorescence and lasing emissions are discussed in Sec. III, and the results of the OB measurements are discussed in Sec. IV.

II. EXPERIMENT

The IOG-2 glass used is doped with 2 wt % Er_2O_3 (1.7×10^{20} ions/cm^3) and codoped with 3 wt % Yb_2O_3 (2.5×10^{20} ions/cm^3). We study lasing and upconversion fluorescent emissions following CW pumping with a tunable 980 nm laser diode (spectral width ~1 nm). IOG-2 glass, with a low glass transition temperature of around 648 K,[19] is ideal for producing microspheres with diameters of between 30 and 70–μm using a microwave plasma torch.[20] A detailed description of our experimental approach has been published elsewhere.[21] Efficient coupling of the pump into the microsphere is attained by using adiabatically tapered fibers fabricated using a direct heating technique.[22] We use a 1-μm-diam, 1550 nm SMF-28 fiber with a typical transmission loss of 0.1 dB/cm. The alignment of taper and microsphere is optimized by adjusting the relative positions of the two, while maximizing the 1550 nm emissions. These lasing emissions are monitored by connecting one end of the fiber taper to an optical spectrum analyzer. During alignment we also monitor the transmission through the fiber and, typically, 10%–15% of the pump light is coupled into the microsphere. All upconversion fluorescence spectra were acquired by free space coupling into an Ocean Optics 2000 spectrometer.

III. LASING AND FLUORESCENCE IN IOG- 2

In our first experiments, we changed the 980 nm pump power from 0 to 10 mW and observed a clear change in the visible emission spectra obtained, as shown in Fig. 1(a) for powers of 2.6 mW, 8.5 mW, and 9.2 mW. These results were obtained for a 50-μm-diam sphere and the chromatic switching behavior is clearly evident at room temperature, by the change in the ratio of the emissions at different wavelengths for the different pump powers. We note three distinct emission bands corresponding to erbium transitions at 520 nm ($^2H_{11/2}\rightarrow{}^4I_{15/2}$), 550 nm ($^4S_{3/2}\rightarrow{}^4I_{15/2}$), and 660 nm ($^4F_{9/2}\rightarrow{}^4I_{15/2}$). The red emission is stronger than red emissions produced in other singly doped glasses investigated in our laboratory, such as Er:ZBLALiP and Er:ZBNA, due to the much larger Yb^{3+} absorption cross section compared to Er^{3+}. One would expect the slope of the fluorescence to exhibit a simple power law dependence, $I_{\text{emission}}\propto I^a_{\text{excitation}}$, where a is the number of pump photons required to produce each emit-

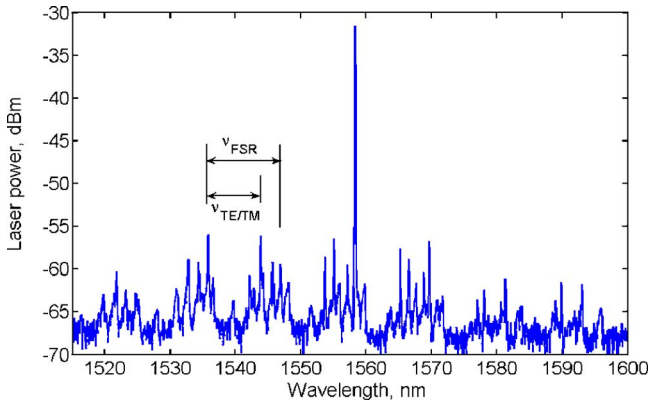

FIG. 2. (Color online) Lasing spectrum and whispering gallery mode structure for a 50-μm-diam IOG-2 microsphere (same as for Fig. 1).

ted photon, thus reflecting the multiphoton nature of the upconversion process. However, this law fails in the presence of OB, as will be shown in Sec. IV. Note that, on occasion, we have also observed a very weak, but distinct, fourth emission band in the UV corresponding to an erbium transition at 405 nm ($^2H_{9/2} \rightarrow {}^4I_{15/2}$). The inset in Fig. 1(a) shows a fluorescence spectrum representing the UV to IR upconversions for a fixed pump power of 8 mW and a 35 μm sphere. Such UV emissions are only observed in spheres that do not lase around 1550 nm, due to a competition between processes involved. We have also monitored the power transmitted past the taper-sphere junction as a function of launched pump power into the fiber taper. This dependency is presented in Fig. 1(b) as the pump power is varied from 0 to 10 mW and back to 0. These measurements allow us to estimate the coupling efficiency of light into the sphere as a function of pump power.

Figure 2 shows the observed IR lasing spectrum around 1550 nm, for the same 50-μm-diam IOG-2 sphere as in Fig. 1, and 10 mW of pump power launched into the fiber taper. A single lasing peak and fluorescing whispering gallery modes are evident. Analysis of the whispering gallery modes in the fluorescence spectrum enables us to measure the free spectral range ν_{FSR} of the sphere modes to be 1.40 THz ($\equiv$11.1 nm). Hence, we can calculate the microsphere diameter using $D=c/(\pi N \nu_{FSR})$, where c is the speed of light in vacuum and N is the refractive index of the material. The refractive index of IOG-2 at room temperature is 1.508 at 1540 nm, yielding a sphere diameter of 45 μm. This agrees reasonably well with an optical microscope measurement of 50$\pm$2 μm. The measured spacing between TE and TM modes of 8.05 nm around 1540 nm agrees well with the calculated value of 8.40 nm. This microsphere has a peak lasing emission of 700 nW for a launched pump power of $\sim$10 mW and, in general, we record lasing thresholds of less than 1 mW.

For ions excited to the $^2F_{5/2}$ level in Yb^{3+}, IOG-2 has a quantum efficiency, $\eta=\lambda_{pump}/\lambda_{laser}$, of about 60%–80%, resulting in the remaining 20%–40% being dissipated in the host matrix as heat. The $^2H_{11/2}$ level and the $^4S_{3/2}$ level can be considered to be in quasithermal equilibrium since the energy gap is $\sim$740 cm^{-1},[23] comparable to the maximum phonon energy of 1300 cm^{-1} for phosphate glass.[12] As such,

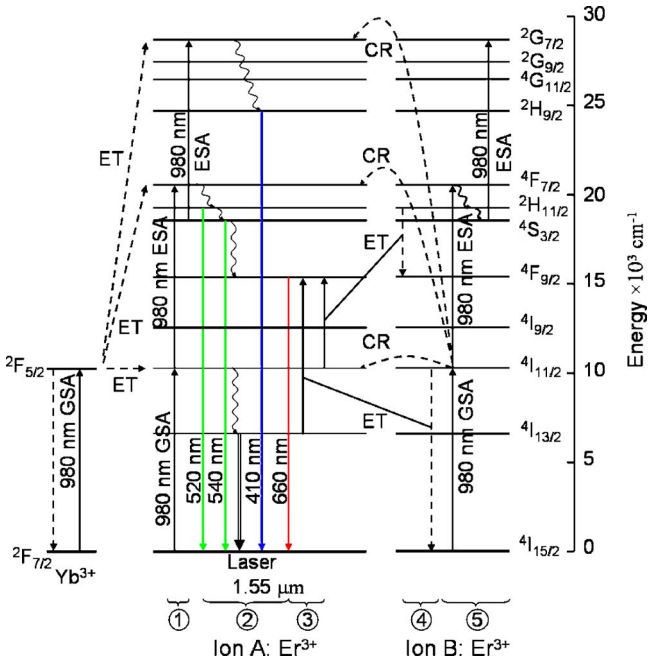

FIG. 3. (Color online) Energy level diagram and fluorescence mechanisms with radiative (solid lines) and nonradiative transitions (wiggly lines). (①) Upconversion based on GSA and ESA in ion A only; (②) radiative and nonradiative decays; (③ and ④) energy transfer processes from ion A to ion B populating the $^4F_{9/2}$ level in ion A; (⑤) GSA and ESA in ion B; (CR) cross relaxation; (ET) energy Transfer; (GSA) ground state absorption; (ESA) excited state absorption.

only one phonon is required to bridge the energy difference between the two green levels, thereby populating the $^2H_{11/2}$ level at room temperature. The thermalization of the $^2H_{11/2}$ level by the $^4S_{3/2}$ level has a temperature-dependent effect on the ratio of the radiative emissions from these two levels as well as the excited state lifetimes.[23] The multiphonon stimulated emission rate between these levels at a temperature T is[24]

$$K_{mp}(T) = K_{mp}(0)\left[1 - \exp\left(-\frac{\hbar\omega}{k_B T}\right)\right]^{-p}, \quad (1)$$

where k_B is Boltzmann's constant, ω is the phonon frequency, and p is the number of phonons required to bridge the energy gap ΔE between the levels and is given by $\Delta E/\hbar\omega$, where $\hbar\omega$ is the phonon energy. For Er-Yb codoped glasses, K_{mp}(295 K) is typically of the order of 10^{11} s^{-1}, which is significantly higher than the value of 10^3 s^{-1} reported for radiative emissions,[24] indicating that the multiphonon decay is dominant. The energy difference between the $^4S_{3/2}$ level and the next lowest level $^4F_{9/2}$, requires three phonons, therefore making this level far less likely to be populated from the $^4S_{3/2}$ level.

The emissions detected from the IOG-2 microsphere, as shown in Figs. 1 and 2, are due to upconversion processes involving multiple pump laser photons and/or lattice phonons. Two upconversion mechanisms which must be considered when trying to understand the origin of the fluorescence results are excited state absorption (ESA) and energy transfer upconversion (ETU).[23,25] These are shown in the energy level diagram in Fig. 3, in which we identify a number of different groups of transition processes, ①–⑤, that play a

role in the generation of the emission spectra. The combination of relatively high cavity quality factor (typically 1×10^7) and strongly localized electromagnetic field in the form of a whispering gallery mode (mode volume $\sim3000\ \mu m^3$) serves to significantly enhance the probability that an excited ion will absorb further pump photons.

Transition groups ① and ⑤ in Fig. 3 are associated with the ground state (GSA) and excited state absorptions in a single erbium ion. As mentioned, there is a resonant energy transfer (ET) from the Yb^{3+} sensitizer ($^2F_{5/2}\rightarrow{}^2F_{7/2}$) to the Er^{3+} ion ($^4I_{15/2}\rightarrow{}^4I_{11/2}$) followed by 980 nm ESA from the $^4I_{11/2}$ level to the $^4F_{7/2}$ level indicated in group ①. Transition group ② deals with the radiative and nonradiative decay processes for a single erbium ion. For example, rapid, nonradiative relaxation from $^4I_{11/2}$ to $^4I_{13/2}$ is possible and falls within this group. In spite of a large energy mismatch of about 1450 cm^{-1} for the $^4I_{13/2}\rightarrow{}^4F_{9/2}$ transition, the long lifetime of the $^4I_{13/2}$ state and associated large population ensures that the ETU mechanism is adequately efficient.[23,26] Due to the close spacing of the $^4F_{7/2}$ and $^4S_{3/2}$ levels, the population of $^4F_{7/2}$ readily decays nonradiatively to the $^4S_{3/2}$ level, whereby the thermal mechanism described previously populates the $^2H_{11/2}$ level. Finally, a second ESA from the $^4S_{3/2}$ level up to the $^2G_{7/2}$ level is followed by nonradiative relaxation down to the $^2H_{9/2}$ level and the subsequent radiative decay to the ground state generates a photon at 410 nm (violet).

At the high concentrations of Er^{3+} and Yb^{3+} in this work the inter ion separation reaches a critically small radius of ~3 nm for Er^{3+} ions and ~2 nm for Yb^{3+} ions. This is close to the value of 2.12 nm for Yb^{3+}-Yb^{3+} ET's and an estimated 1.5–2.0 nm for Yb^{3+}-Er^{3+} ET's as determined from the Förster-Dexter theory,[27,28] dramatically enhancing the probability of Yb^{3+}-Yb^{3+}, Yb^{3+}-Er^{3+} and, presumably, Er^{3+}-Er^{3+} energy transfers. The critical radius R_{sx} is determined by the overlap of the emission and absorption cross sections and is given by

$$R_{sx}^6=\frac{3c\tau_s}{8\pi^4n^2}\int\sigma_{ems}^s(\lambda)\sigma_{abs}^x(\lambda)d\lambda, \tag{2}$$

where c is the velocity of the photons, $\tau_s=1.4$ ms is the fluorescence decay time of the unperturbed sensitizer, n is the refractive index, σ_{ems} is the emission cross section, and σ_{abs} is the absorption cross section. The emission and absorption cross sections are shown in Fig. 4, and are determined from measurements with a bulk sample of IOG-2. The ion s stands for the sensitizer, i.e., the Yb^{3+} ions, and the ion x stands for either the sensitizer or the Er^{3+} acceptor ions. For nonradiative dipole-dipole interactions the energy transfer rate rapidly increases according to the inverse of the ion separation to the sixth power.

A further group ② transition deals with red emissions from a single erbium ion. However, the strength of the observed red emission cannot be wholly explained by multiphonon relaxation from the $^4S_{3/2}$ level to the $^4F_{9/2}$ level, due to the low relaxation rate. Notwithstanding the ESA process already mentioned, two ETU cross-relaxation channels can explain the strength of the red emission relative to the green emissions and the associated processes are indicated by transition groups ③ and ④ in Fig. 3. The first ETU is via $^4I_{11/2}(B)+{}^4I_{13/2}(A)\rightarrow{}^4I_{15/2}(B)+{}^4F_{9/2}(A)$ and the second channel is via $^2H_{11/2}(B)+{}^4I_{11/2}(A)\rightarrow{}^4F_{9/2}(B)+{}^4F_{9/2}(A)$, where A and B denote the two erbium ions involved. Therefore, ions are removed from the green levels and transferred to the red $^4F_{9/2}$ level. The two possible cross-relaxation processes feeding the $^4F_{9/2}$ level deplete the intermediate $^4I_{11/2}$ level and the metastable $^4I_{13/2}$ level, thereby placing the 1.5 μm emission in competition with the red emission and the other upconversion processes. We find that the power of the red emission is, typically, twice as high in microspheres that exhibit no lasing (due to excessive inhomogeneities in the cavity) compared to those that exhibit lasing.

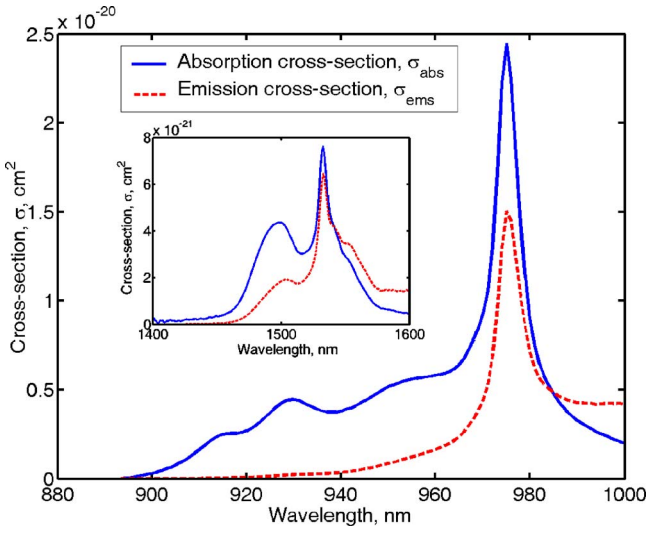

FIG. 4. (Color online) Absorption and emission cross sections for Er^{3+}-Yb^{3+} codoped IOG-2 bulk glass.

IV. RESULTS AND DISCUSSION

A. Intensity switching

In order to study the optical bistability of the microspheres we measured the emission intensity as a function of launched pump power for a single sphere at three different emission wavelengths: 520 nm (green), 660 nm (red), and 1550 nm (IR). The pump power was increased from 0 to 10 mW and back to 0, while recording the fluorescence emission intensities [Fig. 5(a)]. These measurements were taken simultaneously to the transmitted pump power shown in Fig. 1(b). As the launched pump power was increased the emission intensities remained almost constant until a critical power of 8.5 mW was reached [cf. Fig. 5(a)], beyond which a sudden and dramatic rise in emission intensity was observed. Increasing the pump power beyond the critical point caused the emission to level out once more. A subsequent reduction in pump power clearly demonstrates hysteretic behavior and a wide bistable region, where the emission can have two intensity values depending on the history of the input power. The sudden jumps (or intensity switching) between the higher and lower branches of the hysteresis loops are characteristic of the optical bistability of the spheres. A bistable response was also observed for the lasing emission in Fig. 5(b) for the same sphere, but in a slightly different

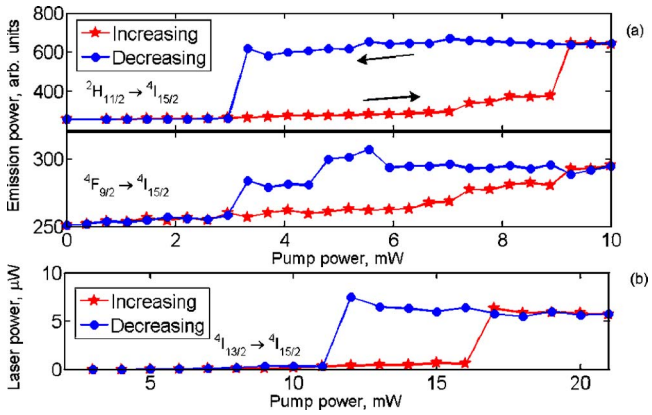

FIG. 5. (Color online) Intensity bistability for green $^2H_{11/2}$ state, red $^4F_{9/2}$ state, and 1.5 μm lasing from the $^4I_{13/2}$ state for a 50-μm-diam sphere. The switching positions for the green and red emissions in (a) differ from the 1.5 μm lasing emission in (b) due to a different setup with a poorer taper-sphere coupling. The corresponding spectra for the visible fluorescence are shown in Fig. 1(a).

experimental setup with the sphere positioned on a different position of the taper. The critical power depends on the taper-sphere coupling efficiency and, hence, differs for the two experiments presented in Fig. 5.

A very promising feature of these microcavity resonators is the high contrast intensity switching observed; the ratio of the relative change in emission powers (defined as the difference between the maximum and minimum powers, divided by the minimum power) is 21 for the green, 11 for the red, and 11 for the IR as determined from Fig. 5. The violet emission is too weak to be considered in these measurements.

B. Chromatic switching

As referred to earlier, the strong temperature dependence in IOG-2 is due to the loss of 20%–40% of the laser power as heat in the glass, in conjunction with its low thermal conductivity. With reference to Fig. 1(b), the sudden dip in transmitted power implies increased pump absorption with an associated increase in the heat generation. In contrast, the sudden increase in transmitted power results in a decrease in heat generation. The increased absorption occurs simultaneously with the sudden rise in the 520 nm ($^2H_{11/2}$) emission intensity as compared to the 550 nm ($^4S_{3/2}$) intensity that was observed when the pump power was increased above the upper switching position of 8.9 mW, as shown in Fig. 1(b). As the pump power was reduced below the lower switching position of 3.3 mW, there was a sudden decrease in intensity ratio due to the drop in pump absorption. Using the methods outlined by Qiao *et al.*,[29] Boltzmann statistics can be used to describe the strong thermal coupling and the population redistribution between the two green levels. The intensity ratio is a function of the internal cavity temperature and is described as[29]

$$\frac{I(^2H_{11/2})}{I(^4S_{3/2})} = \frac{r_H g_H \hbar\omega_H}{r_S g_S \hbar\omega_S} \exp\left(\frac{\Delta E}{k_b T}\right), \tag{3}$$

where I is the integrated emission intensity for a particular level, r is the total spontaneous emission rate, g is the $(2J+1)$ multiplicity (or degeneracy) of each manifold, $\hbar\omega_H(\hbar\omega_S)$ is the energy of level $^4H_{11/2}(^4S_{3/2})$, and ΔE is the energy separation between the levels. According to Eq. (3), as the temperature is increased the $^2H_{11/2}$ level is more efficiently populated and an increasingly larger fraction of the $^4S_{3/2}$ population is rapidly promoted to this upper level and, consequently, the ratio of the emissions from the two states inverts so that the $^2H_{11/2}$ emission becomes stronger. This chromatic switching can yield intensity ratios of up to 2.8 for the integrated power from the 520 nm ($^2H_{11/2}$) and 550 nm ($^4S_{3/2}$) emissions (data not shown). From Eq. (3) this indicates a temperature of 642 K, just below the glass transition value of 648 K.[19] This temperature seems exceptionally high, although there was no evidence of thermal stresses, fracturing of the glass or other defects in the microsphere during these measurements. However, it is important to emphasize that the temperature calculated using this method does not represent the temperature of the entire sphere, but rather the temperature of the mode volume. Heat dissipation from this region through the remainder of the material would account for no evident thermal stress on the sphere itself, which is likely to be at a much lower temperature.

C. Temperature dependence of optical bistability

Previously reported mechanisms for OB in Tm-Yb-doped BaY_2F_8 crystals have suggested that photon avalanche may be a possible mediator, while for silica microspheres the Kerr effect led to OB at 2 K.[30,31] Both these mechanisms are temperature independent. However, other mechanisms such as the thermo-optic effect,[8,18] nonlinear upconversion and energy transfer rates,[32,33] and thermal avalanche[2] are temperature dependent. In order to gain a further understanding on the mechanisms involved, the temperature dependence of the OB was examined by placing a platinum heater and thermocouple close to the microsphere and heating it to around 345 K. The pump power transmitted past the taper-sphere junction was recorded at the same time as the microsphere emissions, while cycling the pump power from low to high and back again as shown in Fig. 6. Comparison of the plots taken at room temperature and at 345 K shows that an increase in external temperature causes the upper knee at 17 mW input power to shift down to 13 mW, while the lower knee at 7 mW only shifts slightly to the right, thereby shortening the bistable region. The pump power was cycled at a slow rate of ~1 mW/min due to the thermal response time of the microsphere. The bistable microsphere emissions are essentially the same as those shown in Fig. 5 except for the different switching positions, and the results shown in Fig. 6 imply that the bistable behavior is a function of temperature.

D. Possible optical bistability mechanisms

In principle, a number of processes may be responsible for the observation of optical bistability, depending on whether the observed effect is temperature dependent or independent. The measurements shown in Fig. 6 indicate clearly that the bistable behavior exhibited by our microspheres is temperature dependent, thereby permitting us to exclude temperature independent processes. Temperature-

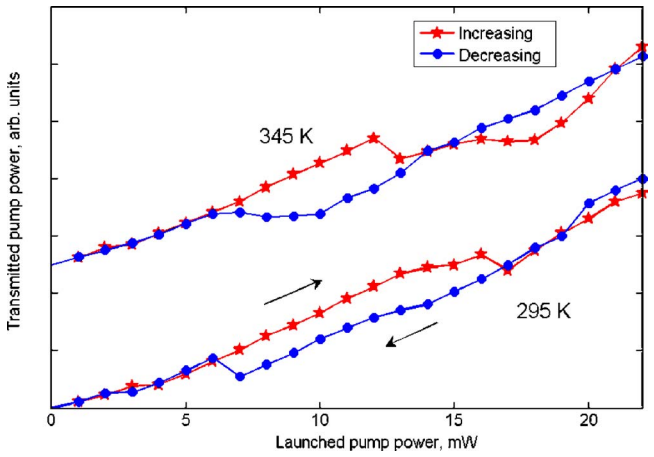

FIG. 6. (Color online) Bistable absorption of pump power at 295 and 345 K for a 50-μm-diam sphere. The data at 345 K has been offset for clarity. As the sphere temperature was increased from 295 K to 345 K, the knee at 17 mW input power shifted to the left, while the lower knee at 7 mW only shifted slightly to the right, thereby shortening the bistable region.

dependent mechanisms that may be responsible include material effects such as (i) strong Yb^{3+}-Yb^{3+} coupling, i.e., nonlinear energy transfer,[32] (ii) nonlinear upconversion rates,[33] and (iii) thermal avalanche,[2] in addition to cavity effects such as (iv) dispersive bistability mediated by the thermo-optic effect.[8,34]

Guillot-Nöel *et al.*[32] have described a mechanism that could be responsible for bistability in the regime of strong Yb^{3+}-Yb^{3+} coupling, in which case cooperative luminescence would be expected. In order to be appreciable, the distance between the ions would need to be of the order of several Å, i.e., significantly smaller than for IOG-2 (21 Å) and, therefore, this effect is unlikely to play a key role. However, if it is present, the luminescence would likely be very weak compared to the single ion Er^{3+} transitions. It is reasonable to assume the back transfer rate is negligible due to the high phonon energy of the host lattice, and is, therefore, unlikely to be the source of nonlinearity in our measurements.

Another possible explanation includes a nonlinear upconversion rate either for Yb^{3+}-Yb^{3+}, Yb^{3+}-Er^{3+}, or Er^{3+}-Er^{3+} energy transfers.[33] This has been observed in high concentration Er^{3+} doped fibers, where the nonlinearity is dependent on population inversion of the lasing levels, and the signal and emission rates. Temperature-dependent effects in the upconversion fluorescence in Er-$YbGa_2S_3$:La_2O_3 chalcogenide glass and germanosilicate optical fibers have been attributed to an exponential increase in the Yb^{3+} absorption cross section elsewhere.[35] However, there have been no reports of bistability relying on these mechanisms.

Thermal avalanche was used to explain bistability in Yb^{3+}-doped bromide lattices by Gamelin *et al.*[2] at cryogenic temperatures. This theory relies on nonlinear absorption in the Yb^{3+} ions with increasing temperature and predicts bistable power absorbance in the microsphere as a function of pump power in the taper, similar to that shown in Fig. 6. As phonons are released into the lattice from Yb^{3+} excited and ground states the temperature increases, thereby increasing absorbance and leading to a further increase in temperature. This cyclic process causes a thermal avalanche for high enough pump power. In order to determine whether thermal avalanche is truly responsible, it would be necessary to perform measurements of the dependence of the Yb^{3+} absorption coefficient and to ascertain whether it is a nonlinear function of internal microsphere temperature above 295 K. However, the results presented in Lei *et al.*[36] for different Yb^{3+}-doped phosphate glasses do not show a suitable nonlinear absorption coefficient necessary for thermal avalanche. This suggests that thermal avalanche theory is also unsuitable to describe the behavior of IOG-2.

We suggest that dispersive bistability[34]—a mechanism commonly used to explain bistability in Fabry-Pérot etalons—can predict our results. The general theory states that as the pump laser frequency is scanned across a high-Q cavity resonance, the cavity intensity rapidly rises, and when the pump frequency moves away from the cavity resonance the cavity intensity rapidly falls. In addition, this description is complicated by the fact that the frequency of the cavity resonance scales approximately linearly with the cavity intensity, leading to a bistable response. In our case, the cavity resonance could be shifted by a temperature-dependent refractive index—the thermo-optic effect—which has a value of $\sim 10^{-6}$/K in phosphate glass.[20] We find that in order to observe bistability the current to the pump laser, and, hence, the pump frequency, need to be adjusted to a precise setting for each sphere. The corollary of this adjustment is the positioning of the laser frequency near a cavity resonance. For the experimental conditions here, a threshold power of about 100 μW in the cavity mode is enough to cause switching—a value which is well below our estimated 10%–15% of pump power coupled into the sphere. Firm evidence of this effect would be possible by probing individual cavity resonances with a narrow linewidth, 980 nm external cavity diode laser, while recording the power transmitted past the taper-sphere coupling junction as described by Rokhsari *et al.*[18]

V. CONCLUSIONS

In conclusion, we have demonstrated a multiwavelength, upconversion, microsphere light source exhibiting optical bistability and we have identified the Er^{3+} transitions and fluorescence mechanisms involved. Factors affecting the dynamics of visible fluorescence and C-band lasing emission have been examined and show that the thermal properties of IOG-2 glass play an important role in the microsphere performance. In particular, the high loss of pump power to the glass as heat, in conjunction with the low thermal conductivity, has a pronounced effect on the green emission from levels $^2H_{11/2}$ and $^4S_{3/2}$. Our calculations show that the close proximity of the ions in our glass greatly enhances the probability of sensitizer-sensitizer and sensitizer-acceptor energy transfers.

We have also reported on the simultaneous observation of chromatic and intensity OB in phosphate glass (Schott IOG-2) at room temperature. These results show that there are two possible temperatures in the bistable region and it is also possible to have two emission intensities for the same excitation power. Chromatic bistability is dependent on the

presence of intensity bistability due to the energy coupling between the green emitting levels $^2H_{11/2}$ and $^4S_{3/2}$. Therefore the switching positions are the same for both types of bistability. The OB shows high contrast switching ratios. The intensity switching shows ratios of 21 for the green, 11 for the red fluorescence emissions, and 11 for the IR lasing, while the chromatic switching ratios $I(^2H_{11/2})/I(^4S_{3/2})$ are as high as 2.8.

We have found that the switching position is dependent on the microsphere temperature, thereby eliminating intensity-dependent mechanisms such as photon avalanche and the Kerr effect. Our observations may be tentatively explained in terms of dispersive bistability, where the temperature-dependent refractive index of phosphate glass causes the resonant cavity mode and the laser mode to behave nonlinearly, yielding a bistable response. Several other possible mechanisms (strong Yb^{3+}-Yb^{3+} coupling, nonlinear upconversion rates, and thermal avalanche) were examined; however, all are considered unfavorable under our experimental conditions.

Microcavity resonators offer substantial miniaturization, greatly reduced power for switching, and allow for all emissions to be easily fiber coupled. In addition, the improved optomechanical properties of IOG-2 compared to other glasses used for OB, such as $CsCdBr_3$, makes this glass appealing for all-optical logic elements in optical engineering applications.

ACKNOWLEDGMENTS

This work was funded by Science Foundation Ireland under Grant No. 02/IN1/128. The authors gratefully acknowledge P. Féron and L. Ghisa from ENSSAT for providing the IOG-2 microspheres. D.O. S. acknowledges support from the Irish Research Council for Science, Engineering and Technology through the Embark Initiative RS/2005/156.

[1] H. M. Gibbs, S. L. McCall, and T. N. C. Venkatesan, Phys. Rev. Lett. **36**, 1135 (1976).
[2] D. R. Gamelin, S. R. Lüthi, and H. U. Güdel, J. Phys. Chem. B **104**, 11045 (2000).
[3] S. M. Redmond and S. C. Rand, Opt. Lett. **28**, 173 (2003).
[4] A. Ródenas, D. Jaque, and J. García Solé, Phys. Rev. B **74**, 035106 (2006).
[5] M. A. Noginov, M. Vondrova, and B. D. Lucas, Phys. Rev. B **65**, 035112 (2001).
[6] T. Hayakawa, H. Ooishi, and M. Nogami, Opt. Lett. **26**, 84 (2001).
[7] A. Kuditcher, M. P. Hehlen, C. M. Florea, K. W. Winick, and S. C. Rand, Phys. Rev. Lett. **84**, 1898 (2000).
[8] V. R. Almeida and M. Lipson, Opt. Lett. **29**, 2387 (2004).
[9] F. Treussart, J. Hare, L. Collot, V. Lefèvre, D. S. Weiss, V. Sandoghdar, J. M. Raimond, and S. Haroche, Opt. Lett. **19**, 1651 (1994).
[10] G. H. Dieke and H. M. Crosswhite, Appl. Opt. **2**, 675 (1963).
[11] M.-F. Joubert, Opt. Mater. **11**, 181 (1999).
[12] P. Laporta, S. Taccheo, S. Longhi, O. Svelto, and C. Svelto, Opt. Mater. **11**, 269 (1999).
[13] E. Snitzer and R. Woodcock, Appl. Phys. Lett. **6**, 45 (1965).
[14] X. Zou and H. Toratani, Phys. Rev. B **52**, 15889 (1995).
[15] S. Jiang, M. Myers, and N. Peyghambarian, J. Non-Cryst. Solids **239**, 143 (1998).
[16] R. Wu, J. D. Myers, M. J. Myers, and C. Rapp, Proc. SPIE **4968**, 11 (2003).
[17] Z. Yang, Z. Feng, and Z. Jiang, J. Phys. D **38**, 1629 (2005).
[18] H. Rokhsari, S. M. Spillane, and K. J. Vahala, Appl. Phys. Lett. **85**, 3029 (2004).
[19] IOG-2 phosphate laser glass specification sheet, Schott Glass Technologies, 400 York Ave., Duryea, PA 18642, USA.
[20] Z. Cai, A. Chardon, H. Xu, P. Féron, and G. M. Stéphan, Opt. Commun. **203**, 301 (2002).
[21] B. J. Shortt, J. Ward, D. O'Shea, and S. Nic Chormaic, Proc. SPIE **6187**, 618708 (2006).
[22] J. C. Knight, G. Cheung, F. Jacques, and T. A. Birks, Opt. Lett. **22**, 1129 (1997).
[23] J. F. Phillips, T. Töpfer, H. Ebendorff-Heiderpriem, D. Ehrt, and R. Sauerbrey, Appl. Phys. B **72**, 399 (2001).
[24] M. P. Hehlen, N. J. Cockroft, T. R. Gosnell, and A. J. Bruce, Phys. Rev. B **56**, 9302 (1997).
[25] M. J. Weber, Phys. Rev. B **8**, 54 (1973).
[26] M. Ajroud, M. Haouari, H. Ben Ouada, H. Mâaref, A. Brenier, and B. Champagnon, Phys. Status Solidi A **202**, 316 (2005).
[27] T. Förster, Ann. Phys. **437**, 55 (1948).
[28] D. L. Dexter, J. Chem. Phys. **21**, 836 (1953).
[29] X. Qiao, X. Fan, M. Wang, J.-Luc Adam, and X. Zhang, J. Phys.: Condens. Matter **18**, 6937 (2006).
[30] M. A. Noginov, M. Vondrova, and D. Casimir, Phys. Rev. B **68**, 195119 (2003).
[31] F. Treussart, V. S. Ilchenko, J.-F. Roch, J. Hare, V. Lefevre-Seguin, J.-M. Raimond, and S. Haroche, Eur. Phys. J. D **1**, 235 (1998).
[32] O. Guillot-Nöel, L. Binet, and D. Gourier, Phys. Rev. B **65**, 245101 (2002).
[33] B. Jaskorzyńska, S. Sergeyev, M. Świllo, and D. Khoptyar, Acta Phys. Pol. A **99**, 147 (2000).
[34] M. M. Mazumder, S. C. Hill, D. Q. Chowdhury, and R. K. Chang, J. Opt. Soc. Am. B **12**, 297 (1995).
[35] E. A. Gouveia, M. T. de Araujo, and A. S. Gouveia-Neto, Braz. J. Phys. **31**, 89 (2001).
[36] G. Lei, J. E. Anderson, M. I. Buchwald, B. C. Edwards, R. I. Epstein, M. T. Murtagh, and G. H. Seigel, IEEE J. Quantum Electron. **34**, 1839 (1998).